Inverse electron-demand Diels-Alder (iEDDA) bioorthogonal conjugation of half-sandwich transition metallocarbonyl entities to a model protein

Daria Jamroz, Nathalie Fischer-durand, Marcin Palusiak, Slawomir Wojtulewski, Szymon Jarzyński, Marlena Stępniewska, Michèle Salmain, Bogna Rudolf

Inverse electron-demand Diels-Alder (iEDDA) bioorthogonal conjugation of half-sandwich transition metallocarbonyl entities to a model protein

Daria Jamroz[1], Nathalie Fischer-Durand[2], Marcin Palusiak[3], Sławomir Wojtulewski[4], Szymon Jarzyński[1], Marlena Puton[1], Michèle Salmain[2], Bogna Rudolf[1,*]

[1]*Department of Organic Chemistry, Faculty of Chemistry, University of Lodz, 91-403 Lodz, Poland*
[2] *Sorbonne Université, CNRS, Institut Parisien de Chimie Moléculaire (IPCM), 75005 Paris, France*
[3]*Department of Physical Chemistry, Faculty of Chemistry, University of Lodz, 90-236 Lodz, Poland*
[4]*Institute of Chemistry, University of Bialystok, Ciolkowskiego 1K, 15-245 Bialystok, Poland*

* To whom correspondence should be addressed ; email: bogna.rudolf@chemia.uni.lodz.pl

Abstract

Novel transition metallocarbonyl complexes carrying a norbornene or an oxanorbornene group were synthesized by [4+2] cycloaddition between the organometallic maleimide dienophiles and cyclopentadiene or furan, respectively. The oxanorbornene adduct was obtained as a mixture of endo and exo isomers as confirmed by X-ray diffraction and NMR spectroscopy. The (oxa)norbornene groups further provided convenient chemical reporters to carry out inverse electron demand Diels-Alder (iEDDA) reactions with tetrazine derivatives. Detailed kinetic studies with a model tetrazine revealed that faster rates of reaction were determined with both isomers of the oxanorbornene complex with respect to the norbornene complexes. Eventually, incorporation of metallocarbonyl entities into bovine serum albumin equipped with tetrazine handles was achieved as shown by IR spectroscopy of the protein conjugates

Keywords

Bioconjugation; infrared spectroscopy, metallocarbonyl complex; tetrazine; norbornene

INTRODUCTION

Among all the bioorthogonal methodologies introduced to date, inverse electron demand Diels-Alder (iEDDA) reactions between 1,2,4,5-tetrazines and alkenes / alkynes appear as one of the most prominent strategies.[1] iEDDA combines high chemoselectivity and fast reaction rates and what is more important, does not require metal catalysis conversely to copper-catalyzed alkyne-azide cycloaddition (CuAAC). This allows reactions to take place in complex media even inside living cells without toxic effects. Furthermore, iEDDA is an irreversible ligation process conversely to normal electron demand D-A reaction owing to the release of dinitrogen during the process through a retro-Diels-Alder reaction (scheme 1). iEDDA is best accomplished using strained and/or electron-rich olefins as dienophiles affording stable dihydropyrizadines in good yield.

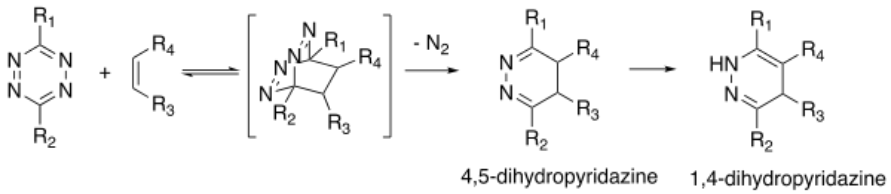

Scheme 1. iEDDA between tetrazine and alkene

Among the various dienophiles reported to date, norbornenes show interesting features as they are easy to synthesize, display very good stability in biological medium and have a relatively small size. Rates of reaction between norbornenes and tetrazines are moderate (second order rate constant in the range of 0.1 $M^{-1}.s^{-1}$ or lower) and highly dependent on electronic, steric and stereomeric factors on the norbornene side.[2]

In our recent efforts to devise bioorthogonal strategies to conjugate transition metallocarbonyl entities to proteins, we first focused our attention on the [3+2] dipolar azide-alkyne cycloaddition (AAC) reaction. To this aim, we designed terminal and strained alkyne (cyclooctyne) derivatives of (η^5-cyclopentadienyl)iron dicarbonyl (Fp) and studied their reaction with a protein carrying azide handles. While the protein was efficiently labeled by copper-catalyzed reaction with the terminal alkyne complex, the uncatalyzed strained alkyne version gave disappointing results because of the unexpected instability of the metallocarbonyl reagent.[3]

Some of us had previously reported the synthesis and characterization of organometallic norbornenes (figure 1) resulting from the Diels-Alder reaction between $CpM(CO)_n(\eta^1$-*N*-maleimidato (M = Fe, n = 2; M = Mo, W, n = 3) complexes as dienophiles and cyclopentadiene.[4] In our hands, metallocarbonyl norbornenes revealed infinitely more stable than metallocarbonyl cyclooctynes. We reckoned that these complexes could be suitable reagents to perform iEDDA reactions with biomolecules carrying the partner tetrazine handle.

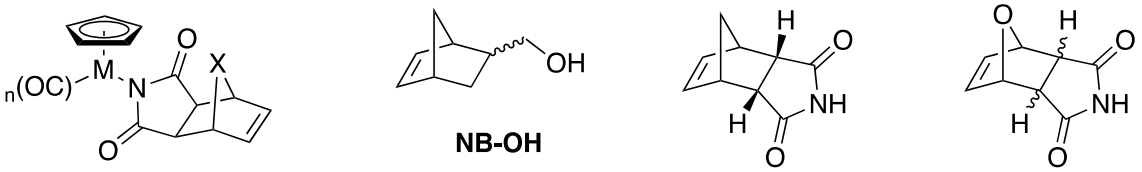

1 M = Fe, n = 2, X = CH_2
2 M = Fe, n = 2, X = O
3 M = Ru, n = 2, X = CH_2
4 M = Mo, n = 3, X = CH_2

Figure 1. Structure of norbornenes used in this study

Surprisingly, literature reports dealing with iEDDA for labeling of biomolecules with transition organometallic complexes are still rather scarce. Recently, Lo and coworkers reported a series of phosphorogenic dipyridyl rhenium(I) tricarbonyl complexes carrying a tetrazine handle on one of the ligands.[5] The same team also reported cyclometalated iridium(III)-based phosphorogenic complexes including a tetrazine group either appended to one of the ligands[6] or directly involved in metal coordination[7].

In this paper we report the synthesis of two new metallocarbonyl norbornenes by Diels-Alder reaction between $[(\eta^5$-Cp)$M(CO)_2(\eta^1$-*N*-maleimidato)] (M = Fe, Ru) and cyclopentadiene or furan (scheme 2). Reactivity studies of all the metallocarbonyl norbornenes were performed on model tetrazine derivatives and bovine serum albumin (BSA) carrying tetrazine handles.

RESULTS AND DISCUSSION

Synthesis of organometallic norbornene and oxanorbornene

Compounds **1** and **4** were synthesized by Diels-Alder reaction between $[(\eta^5$-Cp)$M(CO)_n(\eta^1$-*N*-maleimidato)] (M = Fe, n = 2; M = Mo, n = 3) and cyclopentadiene as previously reported.[4] In both cases, the endo isomer was solely obtained as shown by the molecular structure of **1**.[4] The same stereochemical outcome had been previously

observed for the reaction between cyclopentadiene and maleimide.[8] The preference for the endo isomer results from the process being under kinetic control and the transition state barrier being lower for the endo adduct.[9]

The ruthenium analog **3** was newly prepared using the same procedure from [(η^5-Cp)Ru(CO)$_2$(η^1-*N*-maleimidato)] (Scheme 2). A single product was again obtained which was identified as the endo isomer on the basis of ^{1}H NMR data by comparison with the data of **1**. There was no significant difference between the ^{1}H NMR spectra of **3** and **1**. Two doublets at 1.66 ppm and 1.49 ppm assigned to the protons of the methylene bridge were observed as well as a singlet at 3.28 ppm assigned to the four aliphatic CH protons. Similarly, two doublets were found at 1.43 and 1.61 ppm together with two singlets at 3.17 and 3.23 assigned to the four aliphatic CH protons of **1**. The ^{1}H NMR spectrum of **3** also displayed a singlet at 5.40 ppm for the 5 protons of the Cp ring (4.97 ppm for Fp-NB) and a singlet at 6.03 ppm (5.97 ppm for **1**) assigned to the two protons of the olefin bond.

Maleimides also undergo [4+2] cycloadditions with furan derivatives to afford oxanorbornenes. This provides a simple strategy to protect maleimides as, conversely to the norbornene products, it is a thermally reversible reaction as the retro-Diels Alder reaction of oxanorbornenes occurs at reasonable temperature.[10] The Diels-Alder reaction between **1** and furan was performed under similar experimental conditions (scheme 2). Two addition products - endo and exo isomers were formed in equal proportions as shown by TLC of the reaction mixture. Previously, the Diels-Alder reaction of furan and maleimide also produced a mixture of endo and exo isomers which was explained by similar transition state barriers for the formation of both isomers and the process being under thermodynamic control.[9]

The two stereoisomers were separated by column chromatography. We found that the chemical shift of the protons of carbons C3 (see numbering in Fig. 2) showed the largest difference between the exo and the endo isomers. The signal for the exo isomer was shifted upfield by 0.75 ppm. The differences in the chemical shifts for the other protons were insignificant. The ^{1}H NMR spectra of both isomers showed a characteristic peak around 5 ppm for Cp-H and a singlet at 6.3 ppm (endo) and 6.45 ppm (exo) assigned to the protons of the olefin bond. The chemical shift of the protons of carbons C6 was observed at 5.16 ppm and 5.21 ppm for the exo and endo isomers, respectively.

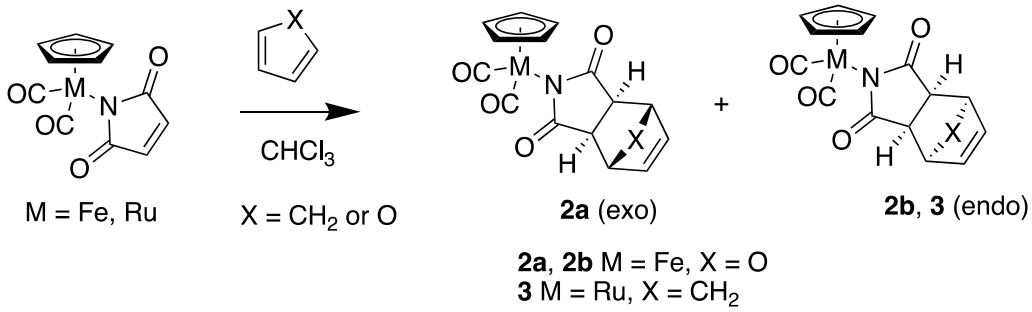

Scheme 2

Crystal structures description

Single crystals of **2a (exo)** and **2b** (**endo)** were obtained after slow evaporation of n-heptane/chloroform (1:3) solution at room temperature.

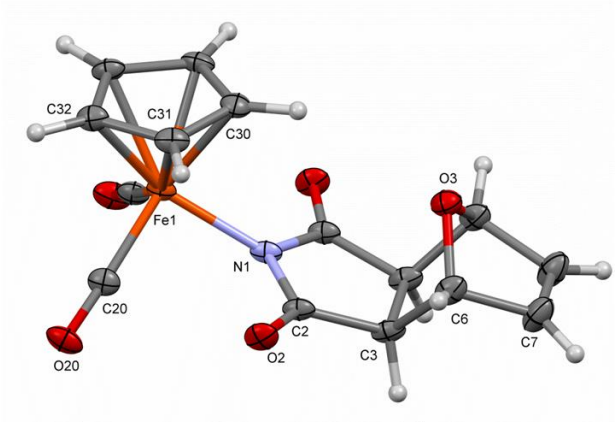

Figure 2. Molecular structure of **2a** (**exo form)** in the crystal. Ellipsoids correspond to 50% probability. Selected bonds (Å) and angles (°) Fe1-C30 2.117(3), Fe1-C31 2.1135(14), Fe1-C32 2.088(2), Fe1-centroid 1.717, Fe1-C20 1.780(2), Fe1-N1 1.959(2), N1-C2 1.374(2), C2-C3 1.512(3), C3-C3a 1.536(4), C3-C6 1.564(3), C6-C7 1.515(3), C7-C7a 1.316(5), C2-O2 1.227(2), C20-O20 1.145(3), C6-O3 1.448(3), Fe1-C20-O20 177.5(2), C2-N1-C2a 110.6(2), Fe1-N1-C2-O2 -10.6(2)

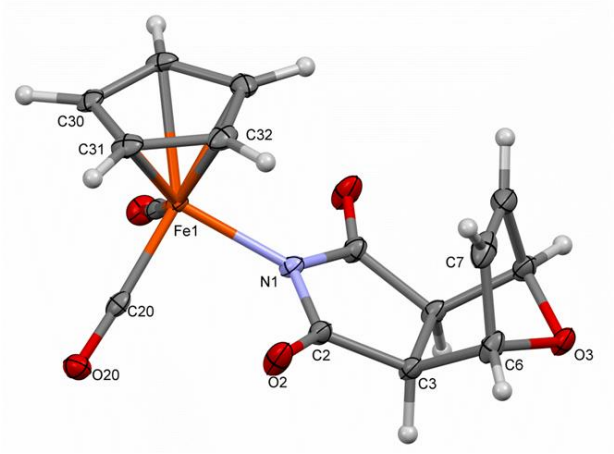

Figure 3. Molecular structure of **2b** (**endo form)** in the crystal. Ellipsoids correspond to 50% probability. Selected bonds (Å) and angles (°) Fe1-C30 2.112(2), Fe1-C31

2.1135(14), Fe1-C32 2.0929(14), Fe1-centroid 1.722, Fe1-C20 1.7873(15), Fe1-N1 1.9624(16), N1-C2 1.3747(17), C2-C3 1.5196(19), C3-C3a 1.536(3), C3-C6 1.564(2), C6-C7 1.519(2), C7-C7a 1.329(4), C2-O2 1.2237(18), C20-O20 1.1422(18), C6-O3 1.4471(17), Fe1-C20-O20 177.12(12), C2-N1-C2a 111.48(16), Fe1-N1-C2-O2 1.1(2)

The molecular structures of **2a** and **2b** are presented in Fig. 2 and Fig. 3. MP: as mentioned in previous comment The asymmetric unit of both crystal structures contains halves of molecular complexes, since the molecules lie on the crystallographic symmetry mirror plane. The Fe1 atom is bonded to the cyclopentadienyl ring (C30-C31-C32-C32a-C31a), two carbonyl ligands (C20-O20 and C20a-O20a) and nitrogen atom N1 of pyrrolidine-2,5-dione ring. The bond lengths between iron atom and the two carbonyl ligands equal 1.780 Å for **2a** and 1.787 Å for **2b**. The distance between iron atom and centroid of the cyclopentadienyl ring equals 1.717 Å and 1.722 Å, respectively. However, the Fe1-N1 bond is significantly longer and equals 1.959 Å (**2a**) and 1.964 Å (**2b**). Hence the overall coordination sphere around iron can be described as a tetrahedron strongly deformed in direction of trigonal pyramid with Fe-Cg apical bond. A similar coordination geometry of iron and other transition metal was found for other cyclopentadienyl complexes previously studied and reported by us.[4, 14, 20, 30, 31] The main difference between the two isomers is the conformation of the oxabicyclo[2.2.1]heptane ring. The conformational change is related to the rotation of the cyclopentadienyl ring. The crystal structure of **2a** contains a molecular complex, where the oxabicyclo[2.2.1]heptane ring is in the exo configuration and the C30-H30 is directed towards the oxygen atom O3 and the distance H30…O3 is 2.821 Å. On the other hand, in the crystal structure **2b** the endo configuration of the oxabicyclo[2.2.1]heptane ring is observed and the cyclopentadienyl ring is rotated by 72 deg [°].

Computational studies

By comparing the energy of *endo* and *exo* isomers of **2** one may find that the *exo* isomer is energetically more favorable by 2.96 kcal/mol. Nevertheless, experimentally, the less energetically favorable *endo* isomer is also observed, which may be explained by general effect of kinetic preference of this isomeric form.[9, 11] For both *endo* and *exo* isomers of **2** there are two possible conformers, that is, *syn* and *anti*, as shown in figure 4. X-ray studies reveal that the *syn* conformation of D-A product is more preferable in solid state conditions.[4] Computational analysis gives the same observation, the molecular energy indicates the *syn* conformer being slightly more stable by 1.73 kcal/mol and 0.53

kcal/mol for *exo* and *endo* isomers, respectively. One possible explanation of this minor energy preference would be the presence of some extra intramolecular interaction in *syn* conformers in respect to its *anti* counterparts. In fact, analysis of electron density distribution allows to find such interactions in *syn* conformers, as shown in Figure 4. Therefore, a bond path with corresponding bond critical point Bader, R.F.W, 1994, *Atoms in Molecules: A Quantum Theory.* USA: Oxford University Press between Cp ligand and the oxanorbornene can be found in *syn* conformer of *exo* isomer.

This type of interaction is well characterized in the literature.[12] The C-H…O bond found in *syn* conformer of *exo* isomer has electron density characteristics typical for other such interactions, with low value of electron density in bond critical point (ρ = 0.005 au) positive values of its laplacian ($\nabla^2\rho$ = 0.018 au) and total electron energy density (H = 0.001au).

In *syn* conformation of endo complex there is also an additional interaction, as indicated by electron density analysis (see Figure 4b). This time it is a weak C-H…π contact, which can also be considered as a specific hydrogen bond with typical interaction electron density characteristics in bond critical point (ρ = 0.006 au, $\nabla^2\rho$ = 0.016 au, H = 0.0007au). It is worth mentioning that C-H… π bonds are for instance responsible for stabilization of acetone crystal in low temperature conditions.[13] Interestingly, merely in the case of conformer *anti* of *endo* isomer there are extra intramolecular contacts between carbonyl groups of Fp entity and carbonyl imide ligand, as shown in Figure 4c. In our previous works, we have shown that these interactions may influence the chemical properties of similar complexes.[4, 14, 15]

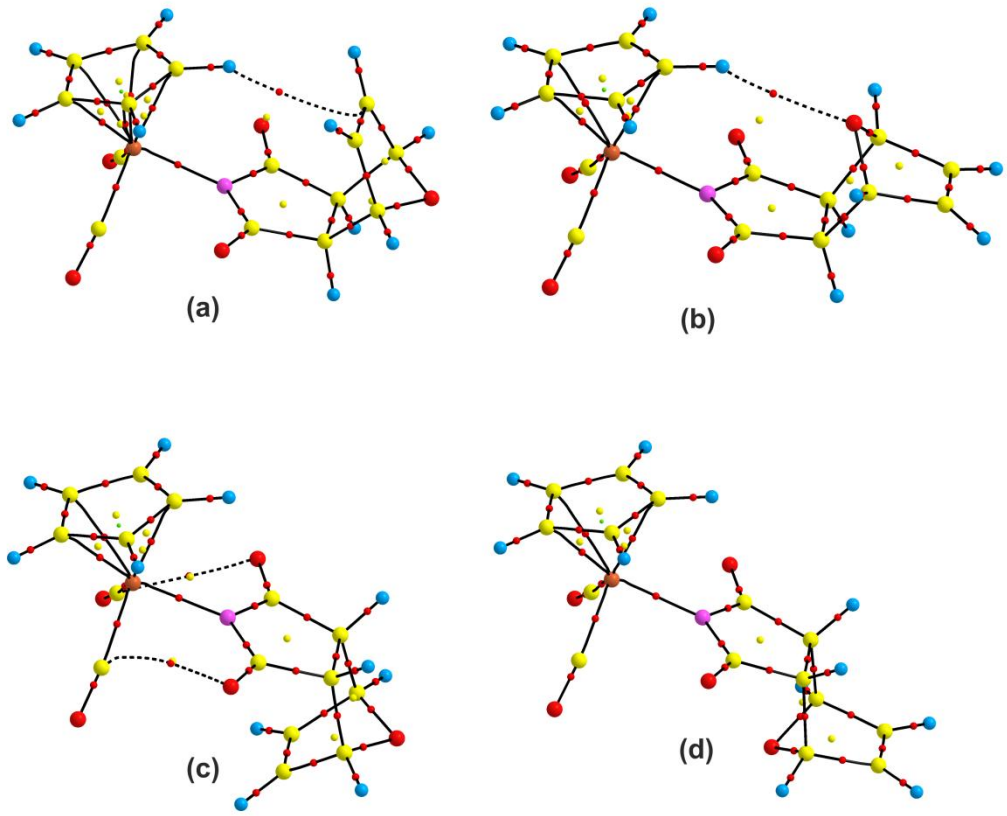

Figure 4**.** Molecular graphs of *syn* (upper side) and *anti* (lower side) conformers of *endo* (left side) and *exo* (right side) isomers of **2**. Larger spheres correspond to atoms (yellow C, red O, pink N, blue H, brown Fe). Small red and yellow spheres are bond and ring critical points. Additional weak interactions discussed in the text are marked with dotted lines (being the proper bond paths). MP: last part of the sentence in brackets

Reactivity studies with model tetrazines

iEDDA reaction between **1** and 3,6-di(phenyl)-1,2,4,5-tetrazine Ph-Tz or 3,6-di(pyridin-2-yl)-1,2,4,5-tetrazine py-Tz was attempted in chloroform. No reaction was observed with Ph-Tz probably owing to its poor reactivity.[16,1]

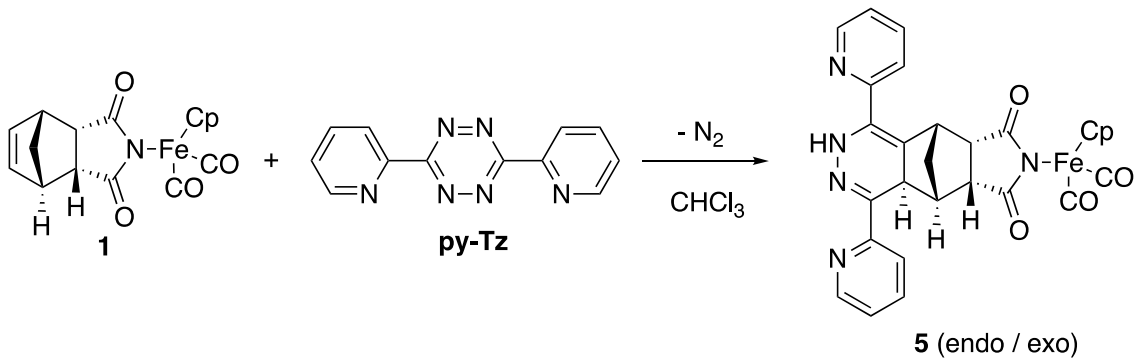

Scheme 3

Conversely, the reaction of **1** and py-Tz (scheme 3) under exclusion of light proceeded steadily at room temperature as the starting complex was fully consumed and the characteristic pink color of py-Tz disappeared, indicating completion of the reaction. Subsequent flash column chromatography afforded pure compound **5** as yellow-green crystals. The structure of **5** was elucidated on the basis of ^{1}H and ^{13}C NMR spectroscopy supplemented with 2D NMR measurements. Only one set of signals is observed on the ^{1}H NMR spectrum in agreement with the formation of a single cycloaddition product (Figure 5). The presence of an unshielded singlet at 9.35 ppm assigned to N-H indicates that the reaction product is a 1,4-dihydropyridazine and not the 4,5-tautomer. The proton carried by C7 at the junction of the dihydropyridazine ring appears as a doublet at 2.23 ppm, with a vicinal coupling constant between H7 and H6 of 1.2 Hz. In consequence, the dihedral angle between both protons is close to 90 deg according to the Karplus equation. This feature is only met for the endo/exo configuration.

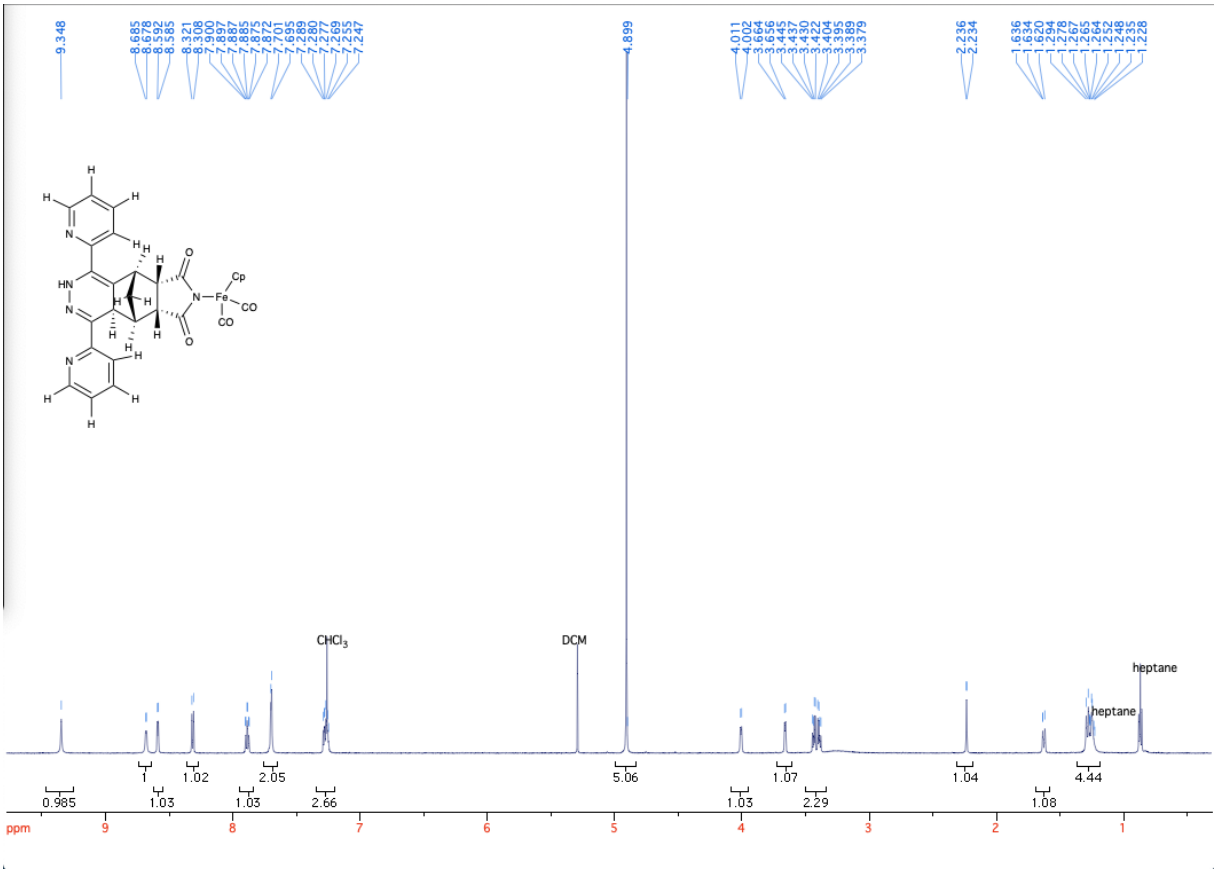

Figure 5. ^{1}H NMR spectrum of **5** in $CDCl_3$

Additional signals in the aromatic region clearly indicated the presence of the two pyridinyl substituents. Moreover, in the ^{13}C NMR spectrum signals found at 40.5 ppm (CH) and 113.3 ppm (C_q) confirmed the formation of the cycloaddition product. The IR spectrum of product **5** displayed typical ν(CO) bands at 1997 and 2047 cm^{-1} owing to the carbonyl ligands of the organometallic moiety.

Kinetic studies

To introduce tetrazine handles onto the model protein BSA, we used the commercially available *N*-hydroxysuccimide ester Tz-NHS depicted in scheme 4 below. Beforehand, the second order rate constants of reaction of the organometallic norbornenes with Tz-NHS were determined under pseudo first-order conditions (i.e. with an excess of dienophile) by monitoring the decrease of absorption of Tz-NHS at 520 nm. This wavelength was preferably chosen over the band at 267 nm (see spectrum below) because of possible interference from the dihydropyridazine products.

Table 1. Second order rate constants of iEDDA reaction between Tz-NHS and various norbornene derivatives

entry	Temperature (K)	Norbornene	Second order rate constant k_{2nd} ($M^{-1}.s^{-1}$)
1	296	Nb-OH[a]	0.77
2	303	Nb-OH[a]	1.7
3	296	**1**[b]	0.006
4	303	**1**[b]	0.012
5	303	**3**[b]	0.0008
6	303	**4**[b]	0.032
7	303	**Suc-NB**[b]	No reaction
8	303	**2a**	0.14
9	303	**2b**	0.063
10	303	**Suc-oxNB**[c]	0.063

[a] mixture of endo and exo isomers; [b] endo isomer; [c] mixure of endo and exo isomers in the proportion 2 to 1

For comparison, the rate of reaction between Tz-NHS and the reference compound 2-norbornene-5-methanol Nb-OH was measured in the same conditions (Table 3, entries 1 and 2). To delineate the influence of the organometallic substituent on the reactivity of the norbornenes, the purely organic succinimide norbornene **Suc-NB** and oxanorbornene **Suc-oxNB** were prepared by reaction of maleimide and cyclopentadiene or furan, respectively following the same reaction condition[4] and their kinetics of reaction with Tz-NHS was measured as well. **Suc-NB** was obtained as a single isomer (endo) whereas **Suc-oxNB** was obtained as a mixture of endo and exo isomers in the proportion 1 to 2.

All the organometallic derivatives gave rise to much slower rates of reaction with respect to Nb-OH. This finding is in agreement with the previously noticed rate reducing ability of electron–withdrawing substituents.[2] The unfavorable endo configuration of the organometallic norbornenes may also play a role in the reduced reactivity of the complexes. There were subtle differences of reactivity among **1** (M=Fe), **3** (M=Ru) and **4** (M=Mo), probably reflecting their relative degree of electron withdrawing strength. Nonetheless, they were still much more reactive than the organic analog **Suc-Nb** for which no reaction was observed after 15 h at 30°C (entry 7). Steric effects were ruled out since the more voluminous complex of the series, that is the molybdenum derivative was also the most reactive.

The rate of reaction between Tz-NHS and the two stereoisomers **2a** and **2b** revealed that this complex was the most reactive of the series of complexes. For instance, the rate constant of **2b** was ca. five times higher than that of **1**. In other words, replacement of the methylene bridge by an oxygen bridge markedly enhanced the reactivity of the Fp derivative. This finding is counterintuitive since the additional electron withdrawing effect of the bridging oxygen should decrease the reactivity of the olefin leading to a smaller rate constant.[17] Conversely to the norbornene series, the rate constant of the organic analog was similar (entry 10).

Moreover, **2a** reacted at a faster rate than **2b** (entries 8 and 9). This is in complete agreement with previous experimental data which had been substantiated by computational calculations on energy barriers.[17] The steric hindrance brought by the

bulky Fp substituent may favor the reaction with the exo isomer. The other reason for the faster reaction rate of the exo isomer **2a** could be the rotation barrier of Fe-N bond which must be larger with respect to **2b** because of C-H…O interaction.

Introduction of tetrazine handles on BSA

A solution of BSA was treated with a 20 molar excess of Tz NHS at pH 7.8 (Scheme 4). After 24 h, the solution was dialysed in PBS to remove unreacted tetrazine. The uv-visible spectrum of the conjugate displays 2 maxima at 526 and 276 nm (Figure 6A). The former one is characteristic of the tetrazine moiety and gives its typical bright pink color. It is slightly shifted to the red compared to the starting tetrazine NHS ester. The tetrazine concentration in BSA-Tz sample was easily deduced from the OD at 526 nm assuming the same extinction coefficient for Tz bound to BSA and Tz-NHS. On the other hand, the protein concentration was measured by the colorimetric BCA assay since the tetrazine is highly absorbing in the 280 nm range. The average coupling ratio was ca. 13 tetrazine entities per BSA.

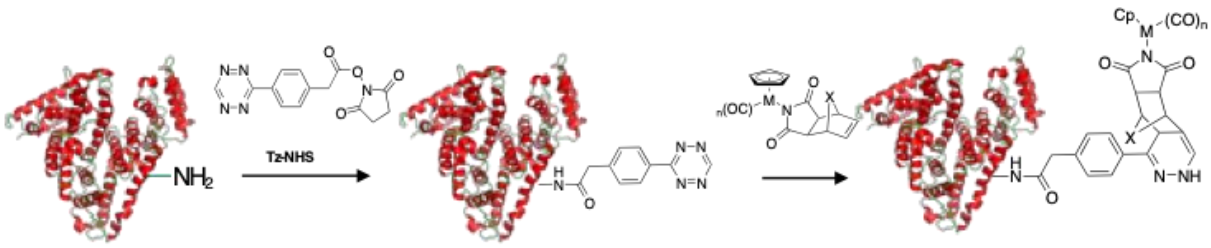

Scheme 4. Introduction of tetrazine handles onto BSA and iEDDA with metallocarbonyl norbornenes

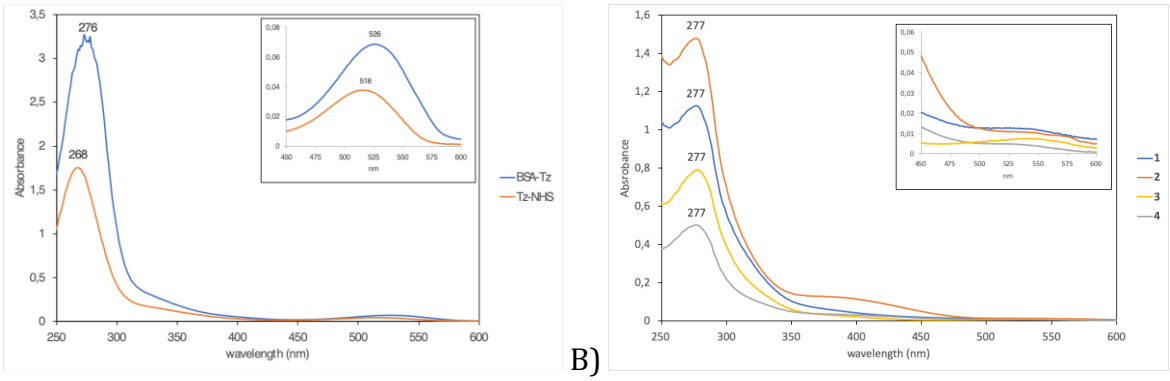

Figure 6 A) uv-visible spectra of Tz-NHS and BSA-Tz conjugate; B) Uv-visible spectra of BSA conjugates after iEDDA with norbornenes

Conjugation of metallocarbonyl norbornenes to BSA-Tz

BSA-Tz was treated with an excess of norbornene with respect to BSA (initial norbornene/Tz ratio = 1.3 to 2) for 17 to 72 h at 30 or 37°C depending on the norbornene (Scheme 4). Unreacted norbornene was removed by extensive dialysis or gel filtration. Solutions were analyzed by uv-visible spectroscopy (figure 6B). A significant change of the uv-vis spectrum of the protein was observed with the disappearance of the characteristic band at 520 nm, except for the reaction product with **3** (see fig. 6B, inset). Solutions were concentrated by centrifugal ultrafiltration and further analyzed by FT-IR spectroscopy by spotting them on nitrocellulose membranes and subsequent air drying (figure 7. The corresponding spectra displayed two bands in the 2000 cm^{-1} region (table 2) characteristic of the metal carbonyl moieties. This indicated that the iEDDA took place between the tetrazine handles and the organometallic norbornenes. This feature and the disappearance of the band at 520 nm are in good agreement with the covalent binding of metal carbonyl groups to BSA by iEDDA.

Table 2. Spectroscopic analysis of BSA conjugates

Complex	IR, v/cm^{-1}	Uv-vis, λ_{max}/nm
1	2050, 2002	277
2a	2051, 2003	277
4	2047, 1962	277
3	2050, 1997	277, 520

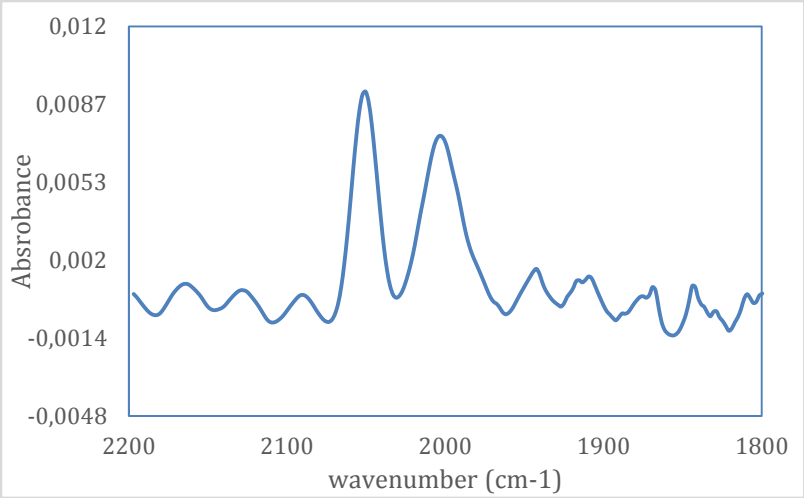

Figure 7. IR spectrum of conjugate resulting from the successive reactions of BSA with Tz-NHS and **1**

The protein content was quantified by the colorimetric BCA assay since the simple protein assay at 280 nm gave overestimated concentration values owing to the significant contribution of the dihydropyridazine entities to the absorbance at 280 nm. Quantification of metallocarbonyl entities was done from the intensity of the higher wavenumber band of each complex measured on the IR spectrum of the conjugates. The average metal-to-BSA ratio equaled 4.8 or 4 after reaction with **1** and **2a**, respectively. For the two other norbornenes **3** and **4**, the coupling ratios were 1.8 and 0.9, respectively.

CONCLUSIONS

In this paper, we demonstrated that various metallocarbonyl reporter entities could be introduced on the model protein BSA by a two-step process, the second one involving the bioorthogonal reaction between tetrazine and norbornene handles. Subtle differences in the reactivity of the metallocarbonyl norbornenes were noticed by carrying kinetic studies with the tetrazine reagent used for further conjugation to BSA, with the oxanorbornene derivative affording the fastest reaction rate with respect to the other organometallic norbornenes. The stereochemistry of the oxanorbornene also influenced the rate of iEDDA, with the exo isomer displaying the fastest rate. The protein bioconjugates were characterized by the presence of bands in the 2000 cm^{-1} spectral range typical of the stretching vibration modes of terminal CO ligands. This bioorthogonal labeling strategy may be further applied to any other biomolecule carrying a tetrazine handle.

EXPERIMENTAL SECTION

Materials and instruments

5-norbornene-2-methanol (mixture of endo and exo isomers) Nb-OH, 3,6-di(pyridin-2-yl)-1,2,4,5-tetrazine and furan were purchased from Aldrich. Cyclopentadiene was obtained by cracking of the dimer (Sigma–Aldrich) directly before use. Complexes [(η^5-Cp)M(CO)$_2$(η^1-*N*-maleimidato)] (M= Fe, Ru) were synthesized as previously described.[18-20] Tetrazine-NHS ester was purchased from Click Chemistry Tools (Scottsdale, AZ, USA). Bovine serum albumin fraction V was purchased from Sigma. Compounds **1** and **4** were synthesized according to a published procedure.[4] Protein concentrations were measured using the micro BCA protein assay kit according to the manufacturer's instructions (Pierce Chemicals). ^{1}H NMR were recorded in $CDCl_3$ on Bruker Avance III (600 Hz) spectrometer. The IR spectra of compounds were recorded in KBr on a FT-IR NEXUS (Thermo Nicolet) spectrometer. ESI-MS spectra were recorded in positive mode on Varian 500-MS LC ion trap spectrometer. All syntheses were carried out under argon. Solvents were dried using standard procedures. Chromatographic purifications were performed on Silica gel Merck 60 (230–400 mesh ASSTM).

Synthetic procedures

Synthesis of 2

To argon-saturated solution of [(η^5-C_5H_5)Fe(CO)$_2$(η^1-*N*-maleimidato)] (100 mg, 0.366 mmol) in methanol/water 1:3 mixture (9 mL), furan (25 mg, 0.366 mmol) was added. The mixture was stirred for 24 h at r.t. The solvent was evaporated and the residue dissolved in chloroform and chromatographed. Yellow bands containing two isomers were eluted with chloroform–MeOH 9:1. The ratio of products was about 1:1 (^{1}H NMR). Crystallization from $CHCl_3$ /heptane (3:1) afforded yellow crystals. **2a:** Yield (33,6%, 42 mg), IR ν/cm^{-1} 2034, 1988 (C≡O) and 1640 (CO imide). ^{1}H NMR (600 MHz, $CDCl_3$) δ/ppm 6.45 (s, 2H, H7), 5.16 (s, 2H, H6), 5.05 (s, 5H, Cp) and 2.80 (s, 2H, H3). ESI-MS m/z 342 $(M+H)^+$. **2b:** (Yield 34,4%,43mg), IR ν/cm^{-1} 2034, 2003 (C≡O) and 1638 (CO imide). ^{1}H NMR (600 MHz, $CDCl_3$) δ/ppm 6.31 (s, 2H, H_{olefin}), 5.21 (s, 2H, COCH), 5.01 (s, 5H, Cp), 3.55 (s, 2H, CH). ESI-MS m/z 364 $(M+Na)^+$

Synthesis of 3

To argon-saturated solution of [(η^5-C_5H_5)Ru(CO)$_2$(η^1-*N*-maleimidato)] (50 mg, 0.157 mmol) in water/methanol 3:1 mixture (9 mL), cyclopentadiene (52 µL, 0.63 mmol) was added. The reaction mixture was stirred for 24 h at r.t. The solvent was evaporated and the residue was dissolved in chloroform and chromatographed. Yellow band containing product was eluted with chloroform–MeOH 9:1. After evaporation of the solvent, the solid was dissolved in chloroform and washed three times with 2.5% aq. NaOH solution. Crystallization from $CHCl_3$ /heptane (3:1) afforded yellow crystals. Yield (66.7%, 40 mg). IR ν/cm^{-1} 2050, 1986 (C≡O) and 1640 (CO). ^{1}H NMR (600 MHz, $CDCl_3$) δ/ppm 6.03 (s, 2H, H_{olefin}), 5.40 (s, 5H, Cp), 3.28 (s, 4H), 1.66 (d, *J* = 8.5 Hz, 1H, CH_2), 1.49 (d, *J* = 8.5 Hz, 1H, CH_2). ESI-MS m/z 386 $(M+H)^+$, 408 $(M+Na)^+$

Synthesis of 5

Compound **1** (100 mg, 0.295mmol), 3,6-di-2-pyridyl-1,2,4,5-tetrazine (70 mg, 0.295mmol) and freshly distilled dry $CHCl_3$ (5 ml) were placed in a round-bottomed flask. The mixture was protected from light, stirred under argon at room temperature and monitored by TLC until the starting materials were fully consumed. Next the solvent was evaporated and crude compound was purified by column chromatography (chloroform/methanol 98:2). Product **5** was crystallized from dichloromethane/heptane to yield yellow-green crystals. Yield (68%, 97 mg). IR ν/cm^{-1} 2050, 1997 (C≡O). ^{1}H NMR (600 MHz, $CDCl_3$) δ/ppm 1.29 (d, $^2J_{HH}$ = 9,5 Hz, 1H, H10), 1.63 (d, $^2J_{HH}$ = 9.5 Hz, 1H, H10`), 2.23 (d, $^3J_{HH}$ = 1.2 Hz, 1H, H7), 3.43 (m, 2H, H6, H9), 3.66 (d, J = 4.7 Hz, 1H, H3), 4.00 (d, J = 5.5 Hz, 1H, H4), 4.91 (s, 5H, Cp), 7.25-7.29 (m, 2H, Ha_{rom}), 7.69 (d, J=3.7 Hz, 2H, H_{arom}), 7.88 (td, J = 7.8, 1.6 Hz, 1H, H_{arom}), 8.31 (d, J = 7.9 Hz, 1H, H_{arom}), 8.59 (d, J = 4.3 Hz, 1H, H_{arom}), 8.68 (d, J = 3.8 Hz, 1H, H_{arom}), 9.35 (s br, 1H, NH,). ^{13}C NMR (150 MHz, $CDCl_3$) δ/ppm 40.5 (CH 2.23 ppm z 1H), 40.6 (CH 4.01 ppm z 1H), 43.7 (CH 3.66ppm z 1H), 45.4 (CH 1.29 i 1.63 ppm z 1H), 51.6 (CH 3.39 ppm z 1H), 52.3 (CH 3.49 ppm z 1H), 84.8 (Cp), 113.3 (Cq), 122.9 (C_{arom}), 123.0 (C_{arom}), 123.2 (C_{arom}), 123.3 (C_{arom}), 133.6 (Cq), 136.6 (C_{arom}), 137.4 (C_{arom}), 138.5 (Cq), 148.3 (C_{arom}), 148.5 (C_{arom}), 150.1 (Cq), 154.0 (Cq), 190.8 (C=O), 191.0 (C=O), 212.3 (C≡O), 212.5 (C≡O). ESI-MS m/z 550 $(M+H)^+$

Synthesis of Suc-NB

To argon-saturated solution of maleimide (50 mg, 0.515 mmol) in methanol/water 1:3 mixture (9 mL), cyclopentadiene (136 mg, 2.0 mmol) was added. The mixture was stirred for 2 h at r.t.. The solvent was evaporated and the residue was dissolved in chloroform and

chromatographed. White band containing product was eluted with chloroform/MeOH 9:1. After evaporation of the solvent the solid was dissolved in chloroform and washed three times with 2.5% aq. NaOH solution. Crystallization from $CHCl_3$ /heptane (3:1) afforded analytically pure sample. Yield (70%, 59 mg). ^{1}H NMR (600 MHz, $CDCl_3$) δ/ppm 6.02 (s, 2H, H_{olefin}) 3.16 (s, 2H, CH-CO), 2.9 (s, 2H, CH), 2.00 (dt, $^3J_{HH}$ =15.7, 2.1 Hz, 1H, CH_2) 1.67 (dt, $^3J_{HH}$ =15.7, 2.8 Hz, 1H, CH_2)

Synthesis of Suc-oxNB

To argon-saturated solution of maleimide (50 mg, 0.515 mmol) in methanol/ water 1:3 mixture (9 mL), furan was added (35 mg, 0.515 mmol). The mixture was stirred for 24 h at r.t.. The solvent was evaporated and the residue dissolved in chloroform and chromatographed. White band containing mixture of isomers was eluted with chloroform–MeOH 9:1. Crystallization from $CHCl_3$ /heptane (3:1) afforded **Suc-oxNB** as a mixture of endo and exo isomers in the proportion 1/2. Yield (70.5%, 60 mg) ^{1}H NMR (600 MHz, MeOD) δ/ppm 6.51 (s, 2H, H_{olefin} endo), 6.56 (s, 2H, H_{olefin} exo) 5.35 (s, 2H, CH-CO endo), 5.16 (s, 2H, CH-CO exo), 3.55 (s, 2H, CH endo), 2.95 (s, 2H, CH exo).

Single crystal X-ray analysis

Suitable crystals were sequentially mounted on a fiber loop and used for X-ray measurement. X-ray data were collected on the Oxford Diffraction SuperNova DualSource diffractometer with use of the monochromated CuKα X-ray source (λ = 1.54184). Crystals were kept at 100 K during data collection. Data reduction and analytical absorption correction were performed with CrysAlis PRO.[26] Using Olex2,[27] the structures were solved with the ShelXS[28] structure solution program using Direct Methods and refined with the ShelXL[28] refinement package using Least Squares minimization. The non-hydrogen atoms were refined anisotropically. Hydrogen atoms were introduced in calculated positions with idealized geometry and constrained using a rigid body model with isotropic displacement parameters equal to 1.2 of the equivalent displacement parameter of the parent atoms. A summary of relevant crystallographic data is given in **Table S1.** The molecular geometry was calculated by Mercury 3.10.[29] The **CCDC 1876957** and **CCDC 1876958** contains the supplementary crystallographic data for this paper. The data can be obtained free of charge from The Cambridge Crystallographic Data Centre via http://www.ccdc.cam.ac.uk/conts/retrieving.html

Methodology of quantum-chemical calculations

Geometry optimization and energy analysis were performed with the Gaussian 09 sets of codes.[21] Calculations were done at ωB97XD[22] level of DFT theory in conjunction with Def2TZVP basis set[23] for all atoms. For all optimized geometries the corresponding WFX files were obtained and used for QTAIM[24] calculations with AIMAll software.[25]

Kinetics of reaction of Tz-NHS with norbornenes

Stock solutions of **1**, **2a** and **2b** (5 mM in PBS), Tz-NHS (10 mM in DMSO), 5-norbornene-2-methanol Nb-OH (mixture of endo and exo-isomers) (100 mM in DMSO), **3** (50 mM in DMSO) and **4** (10 mM in DMSO) were prepared. Mixtures containing Tz-NHS (1 mM) and (oxa)norbornene (4 mM) in PBS/DMSO 9:1 to 1:1 (500 µL) were prepared in a test tube and immediately transferred in a plastic cuvette. The absorption spectrum (600 – 450 nm) was recorded for 15 to 900 min at 20 or 30°C. The OD at 520 nm was plotted as a function of time. Non linear fitting of the data was done assuming first order kinetics, equation (1) where k_{obs} is the pseudo first order rate constant.

(1) $OD_{520} = A + B*\exp(-k_{obs} * t)$

The second order rate constant k_{2nd} was calculated from equation (2).

(2) $k_{2nd} = k_{obs}/[\text{norbornene}]$

Conjugation of tetrazine to BSA

To a solution of BSA (20 mg, 300 nmol) in NaPB pH=7.8 (1 mL), was added a solution of tetrazine-NHS ester (1.89 mg; 6.06 µmol, 20 molar eq.) in DMSO (0.2 mL). The reaction was stirred for 24 h at r.t. and the protein was purified by dialysis in PBS pH 7.4 (1 day), transferred to a centrifugal filter and concentrated to 0.5 mL. The concentration of tetrazine conjugated to BSA was calculated from the absorbance of the conjugate at 520 nm taking ε = 370 $M^{-1}.cm^{-1}$. Protein concentration was assayed by the microBCA method.

Conjugation of 1 to BSA-Tz

To a solution of BSA-Tz in PBS (2.9 mg; 44 nmol; 0.125 mL) was added **1** (0.46 mg, 1.36 µmol; 31 eq.) in PBS (0.375 mL). After stirring for 24 h at 30ºC, the mixture was purified by dialysis in PBS pH 7.4 (1 day), then the solution was transferred to a centrifugal filter (Amicon Ultra – 2 ml, 30 Kda) and concentrated to 0.3 mL. Protein concentration was assayed by the microBCA method.

Conjugation of other norbornenes to BSA-Tz

To a solution of BSA-Tz in PBS (0.9 mg; 13.6 nmol, 0.05 mL) was added a solution of norbornene in DMSO (5 mM; 50 µL; 5 µmol) and the volume was completed to 0.5 mL with PBS. After stirring at 37°C for 17 h (**2a** and **4**) or 72 h (**3**), the mixture was passed on a prepacked gel desalting column (dextran desalting column, 10 mL, Thermo scientific) and species were eluted with PBS. Twelve 1-ml fractions were collected manually and the fractions containing the protein were pooled. The solution was transferred to a centrifugal filter (Amicon Ultra – 2 ml, 30 KDa) and concentrated to 0.3 mL. Protein concentration was assayed by the microBCA method.

Quantification of metallocarbonyl entities by IR spectroscopy

The concentration of metallocarbonyl moieties in conjugate samples was determined by IR analysis according to our previously described procedure and using the following calibration curve equations.

Fp : $y = 25.6\ x + 0.9$ (y in µmol/mL and x = absorbance at 2050 cm^{-1} * 1000)

Rp : $y = 33.3\ x - 0.43$ (y in µmol/mL and x = absorbance at 2050 cm^{-1} * 1000)

Mp : $y = 22.5\ x + 0.09$ (y in µmol/mL and x = absorbance at 2050 cm^{-1} * 1000)

ACKNOWLEDGEMENTS

This work was financially supported by the University of Lodz, Poland, Faculty of Chemistry, CNRS and Sorbonne Université, France and by ERASMUS + programme of the European Union for funding internships in Paris (D. L.). Funding for this research was also provided by EFRD in Operational Programme Development of Eastern Poland 2007–2013 (project No. POPW.01.03.00-20-004/11, for the Oxford Diffraction SuperNova DualSource diffractometer).

Supplementary material

REFERENCES.

1. Oliveira, B. L.; Guo, Z.; Bernardes, G. J. L., Inverse electron demand Diels–Alder reactions in chemical biology. *Chemical Society Reviews* **2017,** *46* (16), 4895-4950.

2. Knall, A.-C.; Hollauf, M.; Slugovc, C., Kinetic studies of inverse electron demand Diels–Alder reactions (iEDDA) of norbornenes and 3,6-dipyridin-2-yl-1,2,4,5-tetrazine. *Tetrahedron Letters* **2014,** *55* (34), 4763-4766.
3. Fischer-Durand, N.; Lizinska, D.; Guérineau, V.; Rudolf, B.; Salmain, M., 'Clickable' cyclopentadienyl iron carbonyl complexes for bioorthogonal conjugation of mid-infrared labels to a model protein and PAMAM dendrimer. *Applied Organometallic Chemistry* **2019,** *0* (0), e4798.
4. Rudolf, B.; Palusiak, M.; Zakrzewski, J., Diels-Alder reaction with cyclopentadiene and electronic structures of (eta(5)-cyclopentadienyl)M(CO)(x)(eta(1)-N-maleimidato) (M = Fe, Mo, W, x=2 or 3). *Journal of Organometallic Chemistry* **2009,** *694* (9-10), 1354-1358.
5. Lo, K. K.-W., Luminescent Rhenium(I) and Iridium(III) Polypyridine Complexes as Biological Probes, Imaging Reagents, and Photocytotoxic Agents. *Accounts of Chemical Research* **2015,** *48* (12), 2985-2995.
6. Li, S. P. Y.; Yip, A. M. H.; Liu, H. W.; Lo, K. K. W., Installing an additional emission quenching pathway in the design of iridium(III)-based phosphorogenic biomaterials for bioorthogonal labelling and imaging. *Biomaterials* **2016,** *103*, 305-313.
7. Tang, T. S. M.; Liu, H. W.; Lo, K. K. W., Monochromophoric iridium(III) pyridyl-tetrazine complexes as a unique design strategy for bioorthogonal probes with luminogenic behavior. *Chemical Communications* **2017,** *53* (23), 3299-3302.
8. Harvey, S. C., Maleimide as a Dienophile. *Journal of the American Chemical Society* **1949,** *71* (3), 1121-1122.
9. Rulíšek, L.; Šebek, P.; Havlas, Z.; Hrabal, R.; Čapek, P.; Svatoš, A., An Experimental and Theoretical Study of Stereoselectivity of Furan−Maleic Anhydride and Furan−Maleimide Diels−Alder Reactions. *The Journal of Organic Chemistry* **2005,** *70* (16), 6295-6302.
10. Discekici, E. H.; St Amant, A. H.; Nguyen, S. N.; Lee, I. H.; Hawker, C. J.; Read de Alaniz, J., Endo and Exo Diels-Alder Adducts: Temperature-Tunable Building Blocks for Selective Chemical Functionalization. *J Am Chem Soc* **2018,** *140* (15), 5009-5013.
11. Johan, F., *Diels-Alder Reaction. In Kirk-Othmer Encyclopedia of Chemical Technology*. John Wiley & Sons, Inc (Ed.). 2016.
12. Grabowski, S. J., What Is the Covalency of Hydrogen Bonding? *Chemical Reviews* **2011,** *111* (4), 2597-2625.
13. K., M. R.; A., K.; P, P., Structures of cubic and orthorhombic phases of acetylene by single-crystal neutron diffraction. *Acta Crystalographica Section B: Structural Science* **1992,** *48*, 726.
14. Rudolf, B.; Salmain, M.; Martel, A.; Palusiak, M.; Zakrzewski, J., eta(1)-N-succinimidato complexes of iron, molybdenum and tungsten as reversible inhibitors of papain. *Journal of Inorganic Biochemistry* **2009,** *103* (8), 1162-1168.
15. Marcin, P., p-Electron Communication Through the Metal Valence Shell – W, Mo and Fe Complexes Containing Maleimidato Moiety *Polish Journal of Chemistry* **2007,** *81* (5-6), 903-909.
16. Knall, A. C.; Slugovc, C., Inverse electron demand Diels-Alder (iEDDA)-initiated conjugation: A (high) potential click chemistry scheme. *Chemical Society Reviews* **2013,** *42* (12), 5131-5142.
17. Vrabel, M.; Kölle, P.; Brunner, K. M.; Gattner, M. J.; López-Carrillo, V.; de Vivie-Riedle, R.; Carell, T., Norbornenes in Inverse Electron-Demand Diels–Alder Reactions. *Chemistry – A European Journal* **2013,** *19* (40), 13309-13312.

18. Rudolf, B.; Zakrzewski, J., (ETA(5)-CYCLOPENTADIENYL)FE(CO)(2)-COMPLEX OF MALEIMIDE ANION - AN ORGANOMETALLIC CARBONYL PROBE FOR BIOMOLECULES CONTAINING HS GROUPS. *Tetrahedron Letters* **1994,** *35* (51), 9611-9612.
19. Rudolf, B.; Palusiak, M.; Zakrzewski, J.; Salmain, M.; Jaouen, G., Sulfhydryl-selective, covalent Labeling of biomolecules with transition metallocarbonyl complexes. Synthesis of (eta(5)-C5H5)M(CO)(3)(eta(1)-N-maleimidato) (M = Mo, W), X-ray structure, and reactivity studies. *Bioconjugate Chemistry* **2005,** *16* (5), 1218-1224.
20. Kubicka, A.; Fomal, E.; Olejniczak, A. B.; Rybarczyk-Pirek, A. J.; Wojtulewski, S.; Rudolf, B., Oxa-Michael reaction of metallocarbonyl complexes bearing the maleimidato ligand. Reactivity studies with selected hydroxy compounds. *Polyhedron* **2016,** *107*, 38-47.
21. M. J. Frisch; G. W. Trucks; H. B. Schlegel; G.; E. Scuseria; M. A. Robb; J. R. Cheeseman; G. Scalmani; V. Barone; B. Mennucci; G. A. Petersson; H. Nakatsuji; M. Caricato; X. Li; H. P. Hratchian; F., A.; Izmaylov; J. Bloino, G. Z., J. L. Sonnenberg, M. Hada, M. Ehara, K. Toyota,; R. Fukuda, J. H., M. Ishida, T. Nakajima, Y. Honda, O. Kitao, H. Nakai,; T. Vreven, J. A. M., Jr., J. E. Peralta, F. Ogliaro, M. Bearpark, J. J.; Heyd, E. B., K. N. Kudin, V. N. Staroverov, R. Kobayashi, J. Normand, K.; Raghavachari, A. R., J. C. Burant, S. S. Iyengar, J. Tomasi, M. Cossi, N.; Rega, J. M. M., M. Klene, J. E. Knox, J. B. Cross, V. Bakken, C. Adamo, J.; Jaramillo, R. G., R. E. Stratmann, O. Yazyev, A. J. Austin, R. Cammi, C.; Pomelli, J. W. O., R. L. Martin, K. Morokuma, V. G. Zakrzewski, G. A.; Voth, P. S., J. J. Dannenberg, S. Dapprich, A. D. Daniels, Ö. Farkas, J.; B. Foresman, J. V. O., J. Cioslowski, and D. J. Fox, Gaussian 09 Revision E. 01. Gaussian, Inc., Wallingford CT: 2009.
22. Chai, J.-D.; Head-Gordon, M., Long-range corrected hybrid density functionals with damped atom–atom dispersion corrections. *Physical Chemistry Chemical Physics* **2008,** *10* (44), 6615-6620.
23. Weigend, F.; Ahlrichs, R., Balanced basis sets of split valence, triple zeta valence and quadruple zeta valence quality for H to Rn: Design and assessment of accuracy. *Phys Chem Chem Phys* **2005,** *7* (18), 3297-305.
24. R. F. W. Bader, *Atoms in Molecules: A Quantum Theory*. USA: Oxford University Press, 1994.
25. A., K. T. *AIMALL program Version 10.12.11*, 10.12.11; 2010.
26. *CrysAlisPro Software system, version 1.171.38.46*, *1.171.38.46*; R*igaku Corporation, Oxford UK*: 2017.
27. Dolomanov, O. V.; Bourhis, L. J.; Gildea, R. J.; Howard, J. A. K.; Puschmann, H., OLEX2: a complete structure solution, refinement and analysis program. *Journal of Applied Crystallography* **2009,** *42* (2), 339-341.
28. Sheldrick, G. M., A short history of SHELX. *Acta Crystallogr A* **2008,** *64* (Pt 1), 112-22.
29. Edgington, P. R.; McCabe, P.; Macrae, C. F.; Pidcock, E.; Shields, G. P.; Taylor, R.; Towler, M.; Van De Streek, J., Mercury: visualization and analysis of crystal structures. *Journal of Applied Crystallography* **2006,** *39* (3), 453-457.
30. Rudolf, B.; Kubicka, A.; Salmain, M.; Palusiak, M.; Rybarczyk-Pirek, A. J.; Wojtulewski, S., Synthesis and characterization of new M(II) carbonyl complexes (M = Fe or Ru) including an eta(1)-N-maleimidato ligand. Reactivity studies with biological thiols. *Journal of Organometallic Chemistry* **2016,** *801*, 101-110.
31. Rudolf, B.; Salmain, M.; Fornal, E.; Rybarczyk-Pirek, A., Metallocarbonyl complexes of bromo- and dibromomaleimide: synthesis and biochemical application. *Applied Organometallic Chemistry* **2012,** *26* (2), 80-85.